Full Length Article

Fracture toughness and sliding properties of magnetron sputtered CrBC and CrBCN coatings

Qianzhi Wang [a,b,c,*], Fei Zhou [a,b,*], Qiang Ma [a,b], Mauro Callisti [d,e], Tomas Polcar [e], Jiwang Yan [f]

[a] State Key Laboratory of Mechanics and Control of Mechanical Structures, Nanjing University of Aeronautics and Astronautics, Nanjing 210016, China
[b] College of Mechanical and Electrical Engineering, Nanjing University of Aeronautics and Astronautics, Nanjing 210016, China
[c] State Key Laboratory of Tribology, Tsinghua University, Beijing 100084, China
[d] Department of Materials Science and Metallurgy, University of Cambridge, Cambridge CB3 0FS, United Kingdom
[e] National Centre for Advanced Tribology at Southampton, Department of Mechanical Engineering, Faculty of Engineering and the Environment, University of Southampton, Southampton SO17 1BJ, UK
[f] Department of Mechanical Engineering, Faculty of Science and Technology, Keio University, Yokohama 2238522, Japan

ARTICLE INFO

ABSTRACT

CrBC and CrBCN coatings with low and high B contents were deposited on 316L steel and Si wafers using an unbalanced magnetron sputtering system. Mechanical properties including hardness (H), elastic modulus (E) and fracture toughness (K_{Ic}) as well as residual stresses (σ) were quantified. A clear correlation between structural, mechanical and tribological properties of coatings was found. In particular, structural analyses indicated that N incorporation in CrBC coatings with high B content caused a significant structural evolution of the nanocomposite structure (crystalline grains embedded into an amorphous matrix) from nc-CrB$_2$/(a-CrB$_x$, a-BC$_x$) to nc-CrN/(a-BC$_x$, a-BN). As a result, the hardness of CrBC coating with high B content decreased from 23.4 to 16.3 GPa but the fracture toughness was enhanced. Consequently, less cracks initiated on CrBCN coatings during tribological tests, which combined with the shielding effect of a-BN on wear debris, led to a low friction coefficient and wear rate.

© 2018 Elsevier B.V. All rights reserved.

1. Introduction

Ceramic materials owing to their excellent heat, corrosion and wear resistances are increasingly being investigated and developed for bearing applications in severe and diverse working conditions [1]. Compared to full ceramic bearings (slider, inner and outer rings are made of ceramics), hybrid bearings (slider is made of ceramics whilst inner and outer rings are made of steel) dominate the market by keeping most of the advantages of full ceramic bearings but at a lower cost [2]. Nevertheless, use of hybrid bearings is still limited by the premature failure of steel rings under some aggressive conditions including corrosive [3,4], abrasive [5,6] or high-speed [7] environments. Moreover, cracking and spallation limited to the near-surface of raceways under rolling/sliding conditions (highly localized stress) is responsible for the failure of rolling bearings [8,9]. It appears clear that surficial properties such as hardness and toughness of raceways are critical aspects to be further enhanced in order to prolong the service life of hybrid bearings. Use of optimized nanocomposite coatings on the inner surface of raceways is an effective approach to improve the performances of hybrid bearings [10,11]. To date, the tribological properties of various coatings including sulfides [12,13], carbides [14], nitrides [15,16] and borides [17–20] were investigated based on their potential application for bearings. Among these, borides such as CrB$_2$ showed promising performances under high load, high speed and high temperature [21]. Even though these coatings presented an attractive hardness ($H \geq 21$ GPa), their high friction coefficient (≥ 0.52 in humid environment) limited their use for industrial applications [22,23]. For this reason, self-lubricant elements such as carbon (up to 17 at.%) was introduced in CrB$_2$ coatings, which effectively reduced the friction coefficient from 0.60 to 0.35. Unfortunately, this CrBC coating was prone to cracking and delamination during tribological tests [24]. Thus, an improvement in the fracture toughness of CrBC coatings is extremely necessary for their bearings applications.

It was reported that, after N incorporation, the fracture toughness of CrB$_2$ coatings was improved from 1.1 to 1.9 MPa$\cdot \sqrt{m}$ [25] while the transverse cracking on CrB$_2$ coatings disappeared [26]. Meantime, the wear rate of CrB$_2$ coatings (3.0×10^{-6} mm^3/Nm) decreased to 2.4×10^{-6} mm^3/Nm [27] and 0.6×10^{-6} mm^3/Nm

* Corresponding authors at: State Key Laboratory of Mechanics and Control of Mechanical Structures, Nanjing University of Aeronautics and Astronautics, Nanjing 210016, China.
   E-mail addresses: qz.wang@nuaa.edu.cn (Q. Wang), fzhou@nuaa.edu.cn (F. Zhou).

[28], respectively. The above results indicate that N incorporation is an effective way of improving the fracture toughness as well as tribological properties of CrB$_2$ coatings. Interestingly, an enhancement in the fracture toughness of CrSiC coatings via N incorporation was shown in our previous work [29]. Therefore, N incorporation is expected to be a potential approach to enhance the fracture toughness and consequently the tribological performance of CrBC coatings. To date, only one study reported the sliding properties of CrBCN coatings in tap water, and authors pointed out that the resultant (H$_3$BO$_3$) between CrBCN coatings and water contributed to superior tribological properties [30]. However, the mechanical properties especially the fracture toughness of CrBCN coatings were not mentioned in ref [30]. Thus, to understand the effect of N incorporation as well as its effects on mechanical properties and wear resistance, further investigations on CrBC(N) coatings are needed.

In this study, the fracture toughness and sliding properties of CrBC and CrBCN coatings against ceramics were investigated. The effect of N incorporation on the fracture toughness of CrBC coatings was elucidated by combining structural and mechanical properties. These were then correlated with the tribological properties of CrBC and CrBCN coatings.

2. Experimental details

2.1. Coatings deposition

CrBC and CrBCN coatings were deposited by using a closed-field unbalanced magnetron sputtering system (UDP-650, Teer Coatings Limited, UK). 316L stainless steel (Ø30 mm × 4 mm, H = 1.8 GPa) with a chemical composition reported in Table 1 and Si wafers (H_s = 12.4 GPa, E_s = 198 GPa, t_s = 525 ± 20 μm) were used as substrates for different purposes. Coatings deposited on Si wafers were used for microstructure analyses while those deposited on steel were used for mechanical and tribological characterizations. Prior to deposition, Ar$^+$ bombardment at a bias voltage of −450 V was used to remove residual contaminants and activate substrates surface. Afterwards, a Cr interlayer (around 200 nm in thickness) was deposited to improve the adhesion between substrate and coating. CrB$_2$ and C targets were sputtered in a pure Ar atmosphere to deposit CrBC coatings while two extra Cr targets were sputtered in a mixed Ar and N$_2$ atmosphere to produce CrBCN coatings. The N$_2$ flow was automatically controlled by an optical emission monitor (OEM) while the compositions of CrBC and CrBCN coatings were controlled by adjusting the corresponding target current. Further details about the deposition processes are listed in Table 2.

2.2. Structural analyses

Structural characterisation of as-deposited coatings was performed by X-ray diffraction (XRD, D8-Advance, Bruker, Germany).

A symmetric scan was conducted in the 2θ range of 20–80° at a constant scanning rate of 10°/min. To confirm chemical bonds as well as accurate chemical composition, CrBC and CrBCN coatings were analyzed by using X-ray photoelectron spectroscopy (XPS, ESCALAB 250, Thermo Scientific). Afterwards, B1s fractal spectrum was deconvoluted by XPS PEAK 4.1 software with the reference C1s peak at 284.8 eV. The thickness and cross-sectional morphology of as-deposited coatings were measured and observed by using a field-emission scanning electron microscope (JEOL-JSM-7001F, Japan). As listed in Table 3, the thickness of CrBC coatings varies from 1.75 to 1.76 μm while that of CrBCN coatings changes from 1.67 to 1.89 μm. TEM samples for CrBC and CrBCN coatings were prepared by using focused ion beam (FIB, NVision 40, Zeiss), where the final polishing was performed with a current of 40 pA at 30 kV to minimize ion beam damage. Subsequently, the lamella was analyzed by a transmission electron microscope (JEM 3010, Japan) operated at 300 kV.

2.3. Mechanical properties

Mechanical properties of as-deposited CrBC and CrBCN coatings were measured by using a Berkovich nanoindenter (ENT-1100a, Elionix Co. Ltd.). Hardness (H) and elastic modulus (E) were determined as an average of at least 36 indents according to the method outlined by Oliver and Pharr [31]. A penetration depth of about 100 nm was set to minimize substrate effects (less than 6% of coatings thickness) [32,33]. Afterwards, plastic work (E_p) was obtained by integrating load-displacement data. Residual stresses (σ) in the as-deposited coatings were quantified by using the sin$^2\psi$ method [34]. Since only Cr (1 1 0) peak exhibited in XRD patterns of all coatings, the stress-free Cr (1 1 0) peak (E = 379.1 GPa, v = 0.128) located at 44.37° was used to calculate residual stress. At each ψ, 2θ value of Cr (1 1 0) was recorded (Fig. 1a) and used to perform the linear regression with sin$^2\psi$ to obtain the slope (M) according to fitting equations (Fig. 1b). Meantime, stress constant (K) of Cr (1 1 0) was calculated according to Eq. (1):

$$K = -\frac{E}{2(1+v)} \times \cot\theta_0 \times \frac{\pi}{180} \qquad (1)$$

where E and v are elastic modulus and Poisson ratio of Cr (1 1 0), θ_0 is stress-free diffraction angle of Cr (1 1 0). Then residual stress (σ) could be obtained according to Eq. (2)

$$\sigma = K \times M \qquad (2)$$

For each ψ angle, 2θ data were recorded in the 2θ range of 44°–47° with a step size of 0.02° (Rigaku Smartlab). A parabolic fitting method, which was manifested to be more reliable in Ref. [35], was adopted to determine the position of broad peaks. However, due to the quite low intensity of Cr (1 1 0) peak at high ψ angles, the top part of Cr (1 1 0) peak higher than 0.3·I$_{max}$ (maximum of intensity) was used in this study.

Table 1
Chemical composition of 316L stainless steel.

Composition	C	Si	Mn	P	S	Ni	Cr	Mo	Fe
Mass fraction (wt%)	0.02	0.65	1.70	0.03	0.01	12.0	17.5	2.5	Balanced

Table 2
Deposition parameters of CrBC and CrBCN coatings.

Coatings	CrB$_2$ target (A)	C target (A)	Cr target (A)	Ar (sccm)	N$_2$ (OEM)	Bias voltage (V)	Rotating speed (rpm)
CrBC-L	4.0	4.0	–	50	–	−80	10
CrBC-H	4.0	2.0	–	50	–	−80	10
CrBCN-L	1.0	4.0	4.0	50	50%	−80	10
CrBCN-H	4.0	4.0	4.0	50	50%	−80	10

Table 3
Thickness and compositions of CrBC and CrBCN coatings.

Coatings	Thickness (μm)	Cr (at.%)	B (at.%)	C (at.%)	N (at.%)
CrBC-L	1.75	23.0 ± 0.5	31.6 ± 0.6	45.4 ± 0.1	–
CrBC-H	1.76	28.6 ± 0.4	35.0 ± 0.5	36.4 ± 0.1	–
CrBCN-L	1.67	34.4 ± 0.3	24.6 ± 0.5	20.4 ± 0.2	20.6 ± 0.4
CrBCN-H	1.89	32.1 ± 0.4	27.2 ± 0.3	22.7 ± 0.3	18.0 ± 0.2
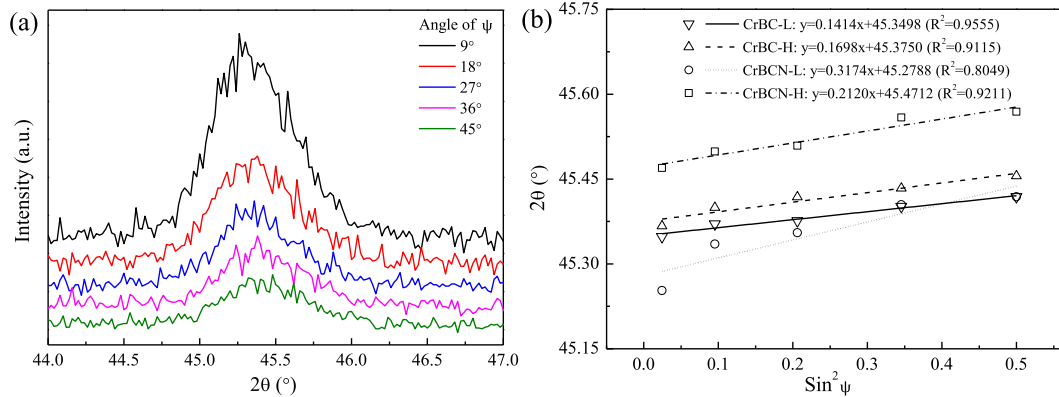
Fig. 1. (a) X-ray diffractograms of CrBC-L coatings at different angles of ψ (b) Liner regressions of CrBC-L, CrBC-H, CrBCN-L and CrBCN-H coatings.

2.4. Fracture toughness

Fracture toughness of the coatings was investigated by nanoindentation. Specifically, five indents at high load (600 mN) were performed on every coating so as to generate cracks. Cracks distribution and size of radial cracks were observed and measured by SEM. Fracture toughness can be obtained via Eq. (3) [36–38]:

$$K_{Ic} = \alpha \left(\frac{E}{H}\right)^{0.5} \left(\frac{P}{C_m^{1.5}}\right) \tag{3}$$

where P is the load (600 mN), H the hardness and E the elastic modulus of the coating under the load P, α is a geometric coefficient related to the shape of tip (0.016 for Berkovich indenter) and C_m is the average length of 15 radial cracks (three radial cracks on each impression and five impressions on each coating). The contour of indents were measured through a laser profilometer (VK-9710, KEYENCE, Japan) by scanning from the indent corner to the midpoint of the opposite edge.

2.5. Tribological test

Ball-on-disk sliding tests were conducted in this study to evaluate the tribological performance of CrBC and CrBCN coatings since this type of test can simulate the tribological conditions typically observed in ball bearings [2]. Based on the potential application of investigated coatings for hybrid bearings, SiC balls (H = 22 GPa, E = 430 GPa) were used as counterpart. The load was set at 3 N, which produced an initial contact pressure (static condition) of 0.73 GPa for CrBC/SiC tribopairs and 0.66 GPa for CrBCN/SiC tribopairs. These contact pressures are comparable to actual bearings contact pressures. The velocity was set to 0.1 m/s over a sliding distance of 500 m necessary to evaluate the friction coefficient in the steady-state regime. During test, the friction force of tribopair was measured by a LMA-A-20N load cell (Kyowa Co. LTD., Japan), which voltage was amplified by a DPM-700B strain amplifier (Kyowa Co. LTD., Japan) and recorded by a NR-110/150 data collection system (Keyence Co. LTD., Japan) connecting with a computer. For each sample, tribological tests were repeated twice, while an additional

test was performed when the relative error on the friction coefficient was over 5%.

The morphology of wear scars on SiC balls was observed by optical microscopy (XJZ-6, China), while SEM (Hitachi S-3400N II, Japan) was used to observe the wear tracks on coatings. The wear volume on coatings was measured by using a non-contact white light interferometer (Micro-XAM™). On this basis, the wear rates were obtained according to the method reported in Ref. [39].

3. Results and discussions

3.1. Microstructure of CrBC and CrBCN coatings

Table 3 summarizes the chemical compositions of sputtered coatings measured by XPS. It was seen that the B concentration in CrBC coatings increased from 31.6 at.% to 35.0 at.% as the current of the C target was decreased from 4.0 to 2.0 A. On the other hand, the B concentration in CrBCN coatings increased from 24.6 at.% to 27.2 at.% when the current of the CrB$_2$ target was increased from 1.0 to 4.0 A. Moreover, owing to additional sputtering from Cr targets during CrBCN depositions, the Cr concentration in CrBCN coatings (32.1–34.4 at.%) was always higher than that in CrBC coatings (23.0–28.6 at.%). To distinguish CrBC and CrBCN coatings with different compositions, coatings containing low (L) and high (H) boron concentrations will be indicated as CrBC-L, CrBC-H, CrBCN-L and CrBCN-H.

XRD patterns for CrBC and CrBCN coatings are illustrated in Fig. 2a. The Cr (110) peak presented at 44.3° in all diffractograms is attributed to the Cr interlayer (JCPDS 06-0694), while the peak located at 69.2° to the Si substrate (JCPDS 27-1402). Two weak peaks at 39.7° and 42.2° are found, which are associated with Cr$_7$C$_3$ compounds (JCPDS 36-1482) due to the diffusion between the interlayer and top layer. A major difference between CrBC-H and CrBCN coatings is the formation of crystalline CrB$_2$ and CrN phases, respectively. In particular, CrBC-H coating exhibited two diffraction peaks at 28.8° and 59.8° related to CrB$_2$ (001) and CrB$_2$ (002) (JCPDS 34-0369), respectively. On the other hand, CrBCN-L and CrBCN-H coatings presented two diffraction peaks
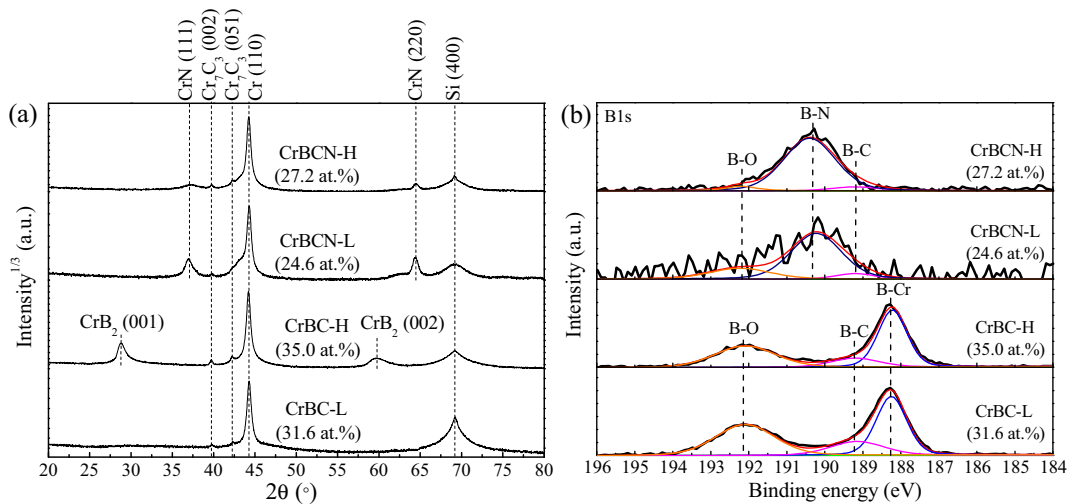
Fig. 2. (a) X-ray diffractograms and (b) B1s XPS fractal spectra of CrBC and CrBCN coatings with different B concentrations.

at 37.0° and 64.5° attributed to CrN (1 1 1) and CrN (2 2 0) (JCPDS 11-0065) [30], respectively. The chemical activity of elements B and N contributes to this result. Namely, element N exhibits a superior ability of drawing electrons to element B, and therefore Cr could relatively easier bond to N than to B after N incorporation. In addition, no B_4C and/or BN phases were detected by XRD, which may indicate that B could exist, in both CrBC and CrBCN coatings, in the form of amorphous BC (a-BC_x) and BN (a-BN).

To confirm the hypotheses about B forms, B1s fractal spectra for CrBC and CrBCN coatings were analyzed (Fig. 2b). The location of main peak for CrBC coatings is rather different from that observed for CrBCN coatings. Specifically, B1s fractal spectra for CrBC coatings was deconvoluted into three peaks located at 188.2 eV, 189.2 eV and 192.1 eV, which are related to B—Cr [40], B—C [41,42] and B—O bonds [41,43], respectively. In contrast, B—N (190.4 eV), B—C and B—O bonds were detected in CrBCN coatings [30]. By combining XRD and XPS (B1s) analyses, it is concluded that in CrBC-L coating B exists in the form of a-CrB_x and a-BC_x. On the other hand, in CrBC-H coating due to the higher B content, B exists in the form of CrB_2, a-CrB_x and a-BC_x. Regarding the CrBCN coatings, B is believed to exist in the form of a-BC_x and a-BN in both CrBCN-L and CrBCN-H coatings due to the absence of B—Cr bonds. As seen in Fig. 3a and b, the through-thickness boundaries of columnar structure are clearly observed in CrBC coatings. In contrast, these boundaries in CrBCN coatings are weakened and even disappear as shown in Fig. 3c and d. It is indicated that the formation of a-BN in CrBCN coatings weakened the columnar structure observed for CrBC coatings, thus resulting in a much more compact and homogeneous structure.

The cross-sectional TEM images in Fig. 4a and d confirmed the formation of a thin (about 50 nm thick) diffusion layer between the Cr bonding layer and CrBC and CrBCN top layers. This diffusion layer was associated with a Cr_7C_3 compound based on XRD analysis (Fig. 2a). SAED analyses reported in the insets in Fig. 4 confirm the formation of hexagonal CrB_2 in CrBC-H coating and the formation of fcc CrN in CrBCN-L coating, which is well consistent with XRD analyses (Fig. 2a). SAED pattern in Fig. 4a shows that, beside the (1 1 0) texture related to the Cr bonding layer, a superimposed texture associated with the $(10\bar{1}1)$ CrB_2 phase with two preferred orientations, i.e. $(10\bar{1}1)$ planes parallel to the substrate and $(10\bar{1}1)$ planes about 60° away from the substrate. According to the crystalline interplanar spacing (0.307, 0.257 and 0.197 nm) of CrB_2 (0 0 0 1), CrB_2 $(10\bar{1}0)$ and CrB_2 $(10\bar{1}1)$, TEM images of CrBC-H coating in Fig. 4b and c show a nanocomposite structure consisting

of CrB_2 (0 0 0 1), CrB_2 $(10\bar{1}0)$ and CrB_2 $(10\bar{1}1)$ crystals embedded in an amorphous matrix (non-feature zone). In contrast, the SAED pattern in Fig. 4d shows much more continuous diffraction rings, thus indicating a much finer polycrystalline structure for CrBCN coating. According to the crystalline interplanar spacing (0.237 and 0.206 nm) of CrN (1 1 1) and CrN (2 0 0), TEM images of CrBCN-L coating in Fig. 4e and f show a nanocomposite structure consisting of CrN (1 1 1) and CrN (2 0 0) crystals embedded in an amorphous matrix.

3.2. Mechanical properties

Mechanical properties measured by nanoindentation are listed in Table 4. Owing to the formation of hard CrB_2 phase, CrBC-H coating presented a relatively high hardness (23.4 GPa). In contrast, CrBCN-L and CrBCN-H coatings presented a relatively low hardness (17.9 and 16.3 GPa) due to the formation of a-BN. Moreover, the separation of CrN nano-grain in CrBCN-H coating was expanded by more a-BN (88.1% a-BN in B1s spectrum) compared to CrBCN-L coating (72.5% a-BN in B1s spectrum). The reinforcing effect of optimal nanocomposite structure on hardness was broken, and therefore CrBCN-H coating exhibited a lower hardness. A similar result was found for CrSiCN coatings for higher Si contents [44]. In principle, the wear resistance of materials is closely dependent on hardness (H). By comparing hardness values listed in Table 4, CrBC-H coating is expected to exhibit the highest wear resistance followed by CrBC-L and CrBCN-L coatings, while CrBCN-H coating should exhibit a poor wear resistance. The actual wear resistance of these four coatings in this study will be presented in Section 3.4 and correlated to their mechanical properties as well as fracture toughness.

3.3. Fracture toughness

Fig. 5 shows the indents produced on every coating along with details of the cracks formed around indents. A long radial crack was observed at the corner of indents produced on CrBC-L and CrBC-H coatings. On the other hand, a short radial crack initiated from the corner of indents produced on CrBCN-L coating. No trace of radial cracks were found on CrBCN-H coating. Based on Eq. (3), fracture toughness (K_{Ic}) of every coating was calculated and listed in Table 4. According to the calculated values, formation of a-BN in CrBCN coating due to N incorporation had positive effects on fracture toughness of CrBC coatings. In the discussion below, we try to
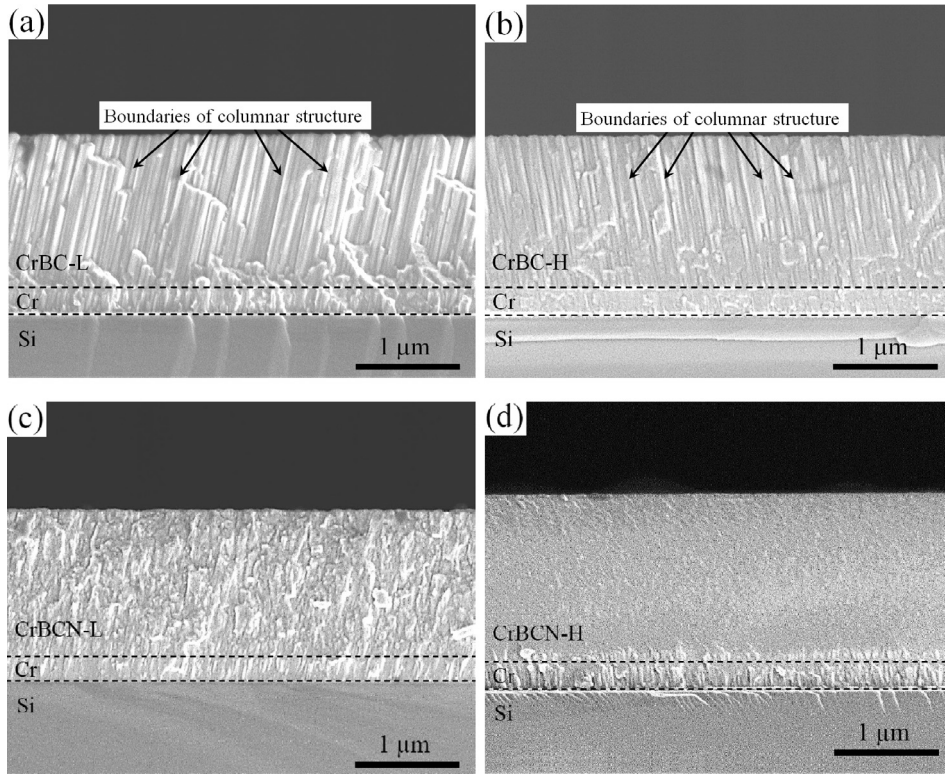
Fig. 3. Cross-sectional morphology of (a) CrBC-L (b) CrBC-H (c) CrBCN-L and (d) CrBCN-H coatings.
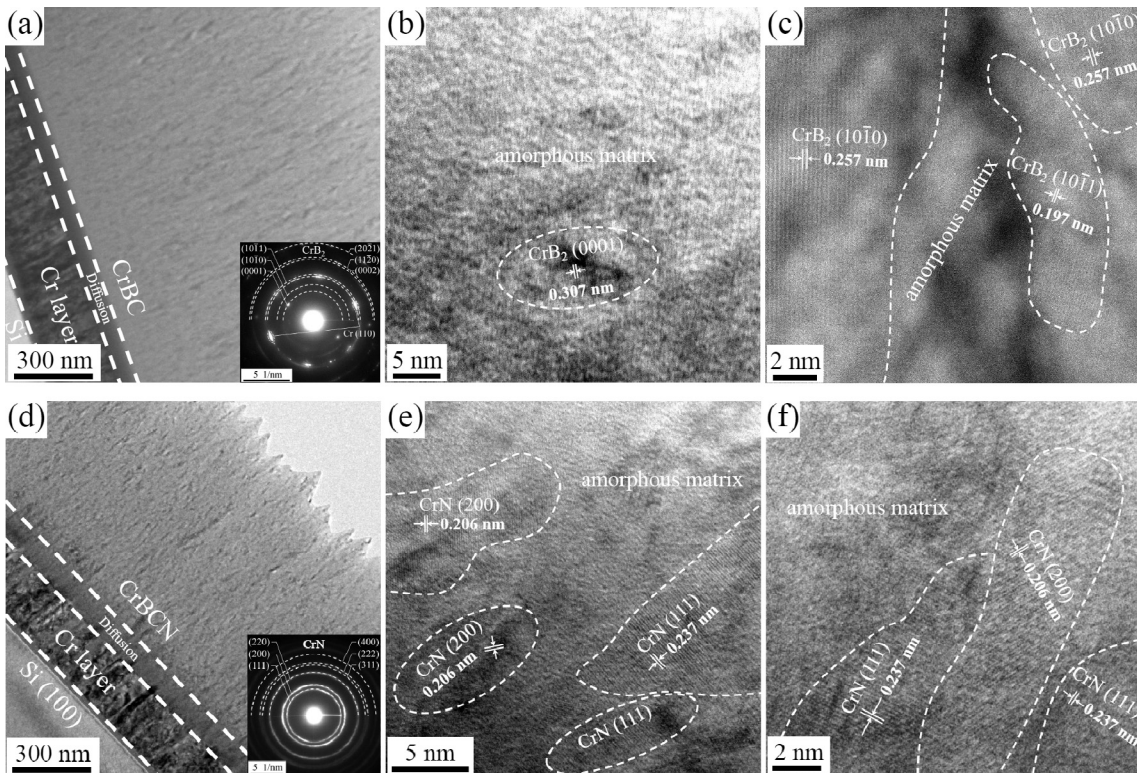

Fig. 4. (a) Cross-sectional morphology with the corresponding SAED and (b) (c) TEM images of CrBC-H coating; (d) cross-sectional morphology with the corresponding SAED and (e) (f) TEM images of CrBCN-L coating.

identify and discuss potential mechanical and structural aspects that contributed at improving the fracture toughness of the investigated coatings. There are expected to be three major factors: (1) H/E ratio, (2) compactness and (3) residual stresses. Musil's group [45–50] reported that in Al–Cu–O, Al–Zr–O and Cu–Zr–O coatings radial cracks were absent for $H/E > 0.1$. It was also pointed

Table 4
Mechanical properties of CrBC and CrBCN coatings.

| Coatings	H (GPa)	E (GPa)	H/E	E_p (pJ)	σ (MPa)	C_m (μm)	K_{Ic} (MPa·$\sqrt{m}$)
CrBC-L	17.7 ± 1.2	295 ± 13	0.060	116.8 ± 8.6	−312	7.96 ± 0.43	2.26 ± 0.25
CrBC-H	23.4 ± 1.5	316 ± 17	0.074	114.0 ± 7.8	−375	7.08 ± 0.70	2.80 ± 0.32
CrBCN-L	17.9 ± 2.3	256 ± 22	0.070	99.5 ± 12.8	−701	6.66 ± 0.54	2.81 ± 0.27
CrBCN-H	16.3 ± 0.8	228 ± 7	0.071	91.9 ± 5.2	−468	No crack	No crack
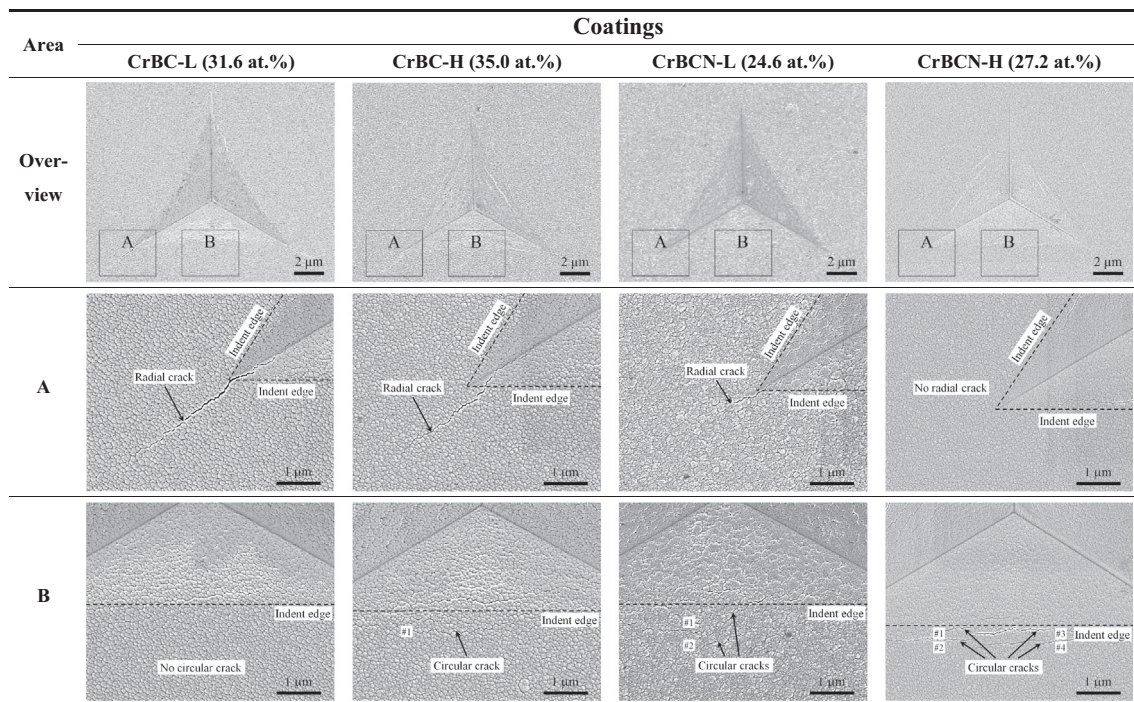
Fig. 5. Overviews and enlarged areas of indent on CrBC and CrBCN coatings with different B concentrations.

out that resistance to radial crack was proportional to H/E. Similar results were also reported in our previous works on CrSiCN (H/E > 0.06) and CrTiAlN coatings (H/E = 0.068) [29,44,51]. Consequently, CrBC-H is expected to be the toughest coating according to the H/E ratios reported in Table 4. However, a longer radial crack was observed on CrBC-H coating compared to CrBCN-L and CrBCN-H coatings (Fig. 5). This finding is attributed to the later two factors mentioned above. In particular, formation of a-BN in CrBCN coatings weakened the columnar structure of CrBC coatings to form a much more compact structure (Fig. 3). Under such a circumstance, radial crack could not propagate along columnar boundaries. In addition, the higher internal compressive stresses found for CrBCN-L and CrBCN-H coatings (−701 and −468 MPa) are believed to offer a strong closing effect against radial cracks [51,52]. Thus, CrBC-H coatings with pronounced columnar structure and low compressive stresses (−375 MPa) facilitated initiation and propagation of radial cracks. Instead, dense CrBCN-H coating with a H/E of 0.71 and an internal compressive stress of −468 MPa exhibited the best resistance against radial cracks.

It is worth mentioning that beside radial cracks, some circular cracks along the edge of indents (Fig. 5) were observed in area B. Musil et al. [45] indicated that circular cracks can easily initiate when hard coatings are deposited on soft substrates. In this study, all of the coatings are much harder than the 316L substrate (1.8 GPa), and therefore circular cracks easily formed. Moreover, CrBCN-L and CrBCN-H coatings exhibited 2 and 4 circular cracks respectively while only one circular crack was found on CrBC-H coating (Fig. 5). Formation of circular cracks was found to be

dependent on three aspects: (1) residual stresses; (2) elastic modulus and (3) plastic work E_p. During the loading process in a nanoindentation test, internal compressive stress in the coating tends to push material towards penetrating tip to form pile-up as shown in Fig. 6. Once a sufficient pile-up is reached, circular cracks form. Pecnik et al. [53] found circular cracks on the pile-up around indents but no circular cracks in the sink-in area around indents. At
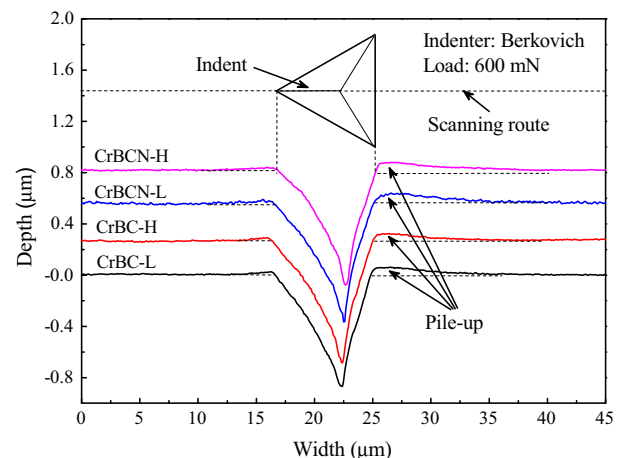
Fig. 6. Contours of indents on CrBC and CrBCN coatings after 600 mN nanoindentation.

the same time, materials with low E exhibit more pronounced bending under the same load. Thus, CrBCN coatings with relatively high compressive residual stresses (−701 and −468 MPa) and low E (256 and 228 GPa) were prone to form circular cracks. Similar results were also reported for Zr—Cu—O coatings [45]. In addition, Wo et al. [54] pointed out that the resistance of coatings to circular crack is proportional to plastic work (E_p). According to E_p values listed in Table 4, CrBCN-L and CrBCN-H coatings should be prone to circular cracks formation, while CrBC-L coating with the highest E_p should exhibit the strongest resistance against circular cracks. This relationship is proven true according to the number of circular cracks observed in Fig. 5.

3.4. Tribological properties

The mean-steady friction coefficient and wear rate of CrBC/SiC and CrBCN/SiC tribopairs are illustrated in Fig. 7a and b. Regardless of B concentration, CrBCN/SiC tribopairs always presented a lower friction coefficient (0.40 and 0.33) and wear rate (3.7×10^{-7} mm^3/Nm and 2.4×10^{-7} mm^3/Nm) than CrBC/SiC tribopairs (0.42 and 0.47; 11.3×10^{-6} mm^3/Nm and 3.2×10^{-6} mm^3/Nm). These results are attributed to the differences in both microstructure and crack resistance. On one hand, formation of the CrB$_2$ hard phase in CrBC coatings acted as abrasive particles during tribological tests, thus leading to rough sliding surfaces and therefore increased friction coefficient and wear rate. Meantime, the low fracture toughness (K_{Ic}) found for CrBC coatings led to pronounced cracks formation during tribological tests, which also contributed at increasing the roughness of sliding surfaces. These aspects are demonstrated by the rough morphology found across the entire sliding surface of SiC balls shown in Fig. 8a and b. In contrast, a-BN matrix in CrBCN coatings could effectively shield wear debris [55]. In addition, due to the higher fracture toughness of CrBCN coatings less cracks were expected to initiate during tribological
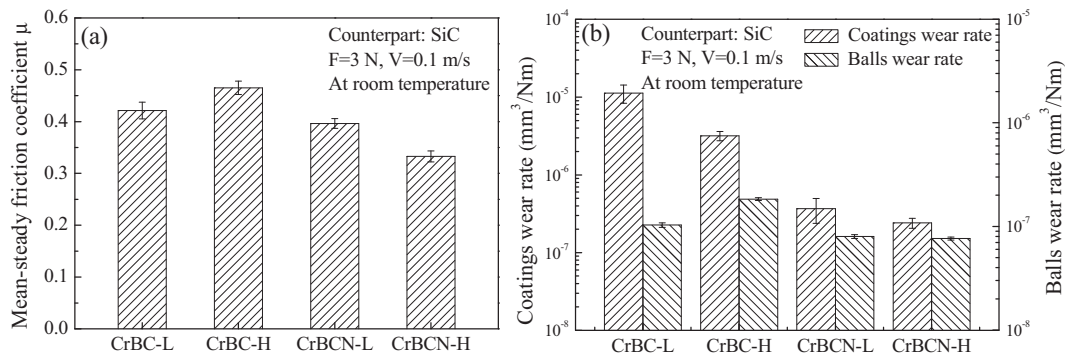

Fig. 7. (a) Mean-steady friction coefficient and (b) wear rates of CrBC/SiC and CrBCN/SiC tribopairs.
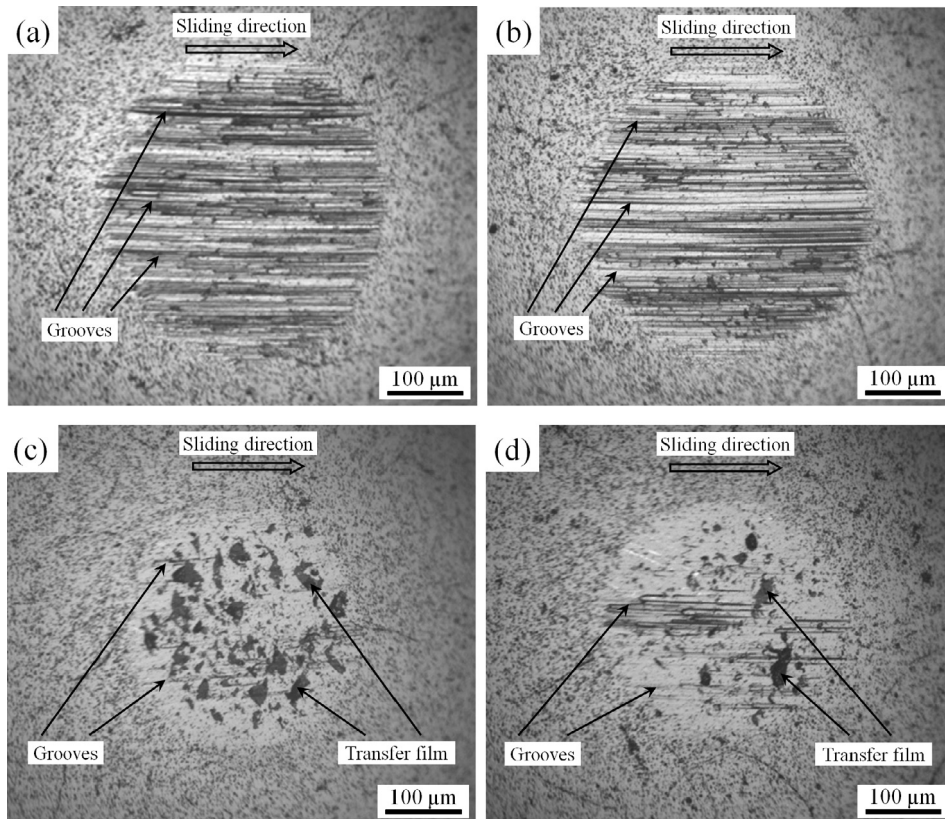

Fig. 8. Optical images of wear scars on SiC balls sliding against (a) CrBC-L (b) CrBC-H (c) CrBCN-L (d) CrBCN-H coatings.

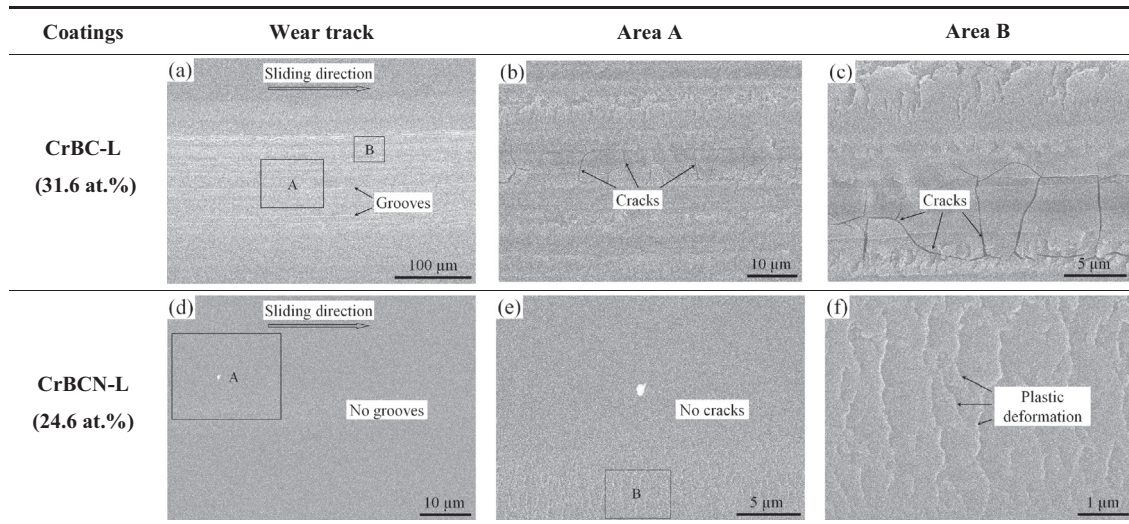| Coatings	Wear track	Area A	Area B
CrBC-L (31.6 at.%)	(a)	(b)	(c)
CrBCN-L (24.6 at.%)	(d)	(e)	(f)

Fig. 9. SEM images of wear tracks on (a) (b) (c) CrBC-L and (d) (e) (f) CrBCN-L coatings.

tests. As a consequence, low friction coefficient and wear rate were attained and attributed to smoother sliding surfaces of SiC balls as shown in Fig. 8c and d.

According to the hardness values listed in Table 4, CrBC-L coating should exhibit comparable wear rate than that exhibited by CrBCN coatings. However, as shown in Fig. 7b, CrBCN-L and CrBCN-H coatings exhibited a much lower wear rate compared to CrBC-L and CrBC-H coatings. This suggests that beside hardness, fracture toughness (K_{Ic}) also plays a role on the wear resistance of CrBC and CrBCN coatings. As seen in Fig. 9a, some obvious grooves parallel to the sliding direction were observed on the wear track of CrBC-L coating. In addition, some consecutive cracks were found in the central part of wear track (Fig. 9b and c) due to the weak fracture toughness of CrBC-L coating. In contrast, no cracks but only plastic deformation was observed on the wear track of CrBCN-L coating (Fig. 9e and f). The morphology of wear track on CrBCN-H coating was exceedingly smooth to distinguish any topographic feature, and no corresponding image were illustrated here. To summarize the wear behaviour, cracking and peeling off during tribological tests caused an increase in wear rate for both CrBC-L and CrBC-H coatings. Instead, the CrBCN-H coating with the highest fracture toughness exhibited the strongest wear resistance. Interestingly, the tribological performance of CrBC and CrBCN coatings was found to be more closely related to their resistance to radial cracks rather than to that against circular cracks. However, further work is needed to clarify this latter aspect.

4. Conclusions

This study investigated possible correlations between structural, mechanical and tribological properties of CrBC and CrBCN nanocomposite coatings. Relevant conclusions are drawn as follows:

(1) N incorporation caused a structural evolution for CrBC-H coating (35.0 at% B) from nc-CrB$_2$/(a-CrB$_x$, a-BC$_x$) to nc-CrN/(a-BC$_x$, a-BN).
(2) N incorporation significantly improved the fracture toughness of CrBC-L coatings (radial crack disappeared) without large changes in hardness (slight drop from 17.7 to 16.3 GPa) compared to CrBCN-H coatings.
(3) CrBCN-H coatings (27.2 at.% B) exhibited low friction coefficient (0.33) and wear rate (2.4×10^{-7} mm^3/Nm) owing to formation of a a-BN phase and enhanced fracture toughness.

(4) Although the hardness of CrBCN-H coating was the lowest, its best toughness contributed to superior tribological performances, which make this coating a promising candidate to be used for fabricating hybrid bearings.

References

[1] H. Takebayashi, in: S. Somiya, F. Aldinger, N. Claussen, R.M. Spriggs, K. Uchino, K. Koumoto, M. Kaneno (Eds.), Handbook of Advanced Ceramics, Academic Press, Waltham, Massachusetts, 2003, pp. 313–331 (Chapter 3.4).
[2] M. Herrmann, in: S. Somiya, R. Danzer, S.W. Freiman, P. Greil, M. Herrmann, M. Kaneno, K. Komeya, T. Ohji, E. Yasuda (Eds.), Handbook of Advanced Ceramics, second ed., Academic Press, Waltham, Massachusetts, 2013, pp .301–328 (Chapter 3.4).
[3] P. Lan, J.L. Meyer, B. Vaezian, A.A. Polycarpou, Advanced polymeric coatings for tilting pad bearings with application in the oil and gas industry, Wear 354–355 (2016) 10–20.
[4] K. Zhang, Effects of test conditions on the tribological behaviour of a journal bearing in molten zinc, Wear 259 (2005) 1248–1253.
[5] J.A. Rodriguez, J.M. Rodriguez, J.C. Garcia, J.A. Arellano, J.L. Maldonado, Diamond like carbon coating of ball bearings for raceway surface by triboadhesion, Indian J. Eng. Mater. Sci. 21 (2014) 104–110.
[6] D. Klaffke, E. Santner, D. Spaltmann, M. Woydt, Influences on the tribological behaviour of slip-rolling DLC-coatings, Wear 259 (2005) 752–758.
[7] A. Igartua, J. Laucirica, A. Aranzabe, T. Leyendecker, O. Lemmer, G. Erkens, M. Week, G. Hanrath, Application of low temperature PVD coatings in rolling bearings: tribological tests and experiences with spindle bearing systems, Surf. Coat. Technol. 86–87 (1996) 460–466.
[8] S. Stewart, R. Ahmed, Rolling contact fatigue of surface coatings-a review, Wear 253 (2002) 1132–1144.
[9] Y. Guo, S. Sun, X. Wu, J. Na, R. Fung, Experimental investigation on double-impulse phenomenon of hybrid ceramic ball bearing with outer race spall, Mech. Syst. Signal Process. (2016), https://doi.org/10.1016/j.ymssp.2016.07.042.

[10] F. Grun, I. Godor, W. Gartner, W. Eichlseder, Tribological performance of thin overlays for journal bearings, Tribol. Int. 44 (2011) 1271–1280.

[11] O. Fukumasa, K. Osaki, S. Fujimoto, C.P. Lungu, A.M. Lungu, Low friction coatings prepared by high performance type spray gun, Surf. Coat. Technol. 169–170 (2003) 415–418.

[12] H. Heshmat, P. Hryniewicz, J.F. Walton II, J.P. Willis, S. Jahanmir, C. DellaCorte, Low-friction wear-resistant coatings for high-temperature foil bearings, Tribol. Int. 38 (2005) 1059–1075.

[13] T. Hirayama, N. Hishida, H. Ishida, H. Yabe, Performances of journal bearing with MoS_2-shot coating for spindle of magnetic recording storage system, Microsyst. Technol. 11 (2005) 751–757.

[14] K. Zhang, L. Battiston, Sliding wear of various materials in molten zinc, Mater. Sci. Technol. 18 (2002) 1551–1560.

[15] M.D. Drory, R.D. Evans, Deposition and characteristics of chromium nitride thin film coatings on precision balls for tribological applications, Surf. Coat. Technol. 206 (2011) 1983–1989.

[16] E.E. Vera, M. Vite, E.A. Gallardo, J.R. Laguna-Camacho, Fatigue life of TiN and CrN coatings in rolling contact, Proc. Inst. Mech. Eng. J: J. Eng. Tribol. 227 (2012) 339–348.

[17] E.E.V. Cardenas, R. Lewis, A.I.M. Perez, J.L.B. Ponce, F.J.P. Pinal, M.O. Domınguez, E.D.R. Arreola, Characterization and wear performance of boride phases over tool steel substrates, Adv. Mech. Eng. 8 (2016) 1–10.

[18] B. Selcuk, R. Ipek, M.B. Karamys, A study on friction and wear behaviour of carburized, carbonitrided and borided AISI 1020 and 5115 steels, J. Mater. Process. Technol. 141 (2003) 189–196.

[19] B.S. Unlu, E. Atik, Investigation of tribological properties of boronised pure Cu journal bearings, Surf. Eng. 26 (2010) 173–177.

[20] S. Taktak, Tribological behaviour of borided bearing steels at elevated temperatures, Surf. Coat. Technol. 201 (2006) 2230–2239.

[21] S.C. Singhal, A hard diffusion boride coating for ferrous materials, Thin Solid Films 45 (1977) 321–329.

[22] M. Audronis, P.J. Kelly, R.D. Arnell, A. Leyland, A. Matthews, The structure and properties of chromium diboride coatings deposited by pulsed magnetron sputtering of powder targets, Surf. Coat. Technol. 200 (2005) 1366–1371.

[23] K.P. Budna, P.H. Mayrhofer, J. Neidhardt, E. Hegedus, I. Kovacs, L. Toth, B. Pecz, C. Mitterer, Effect of nitrogen-incorporation on structure, properties and performance of magnetron sputtered CrB_2, Surf. Coat. Technol. 202 (2008) 3088–3093.

[24] N. Nedfors, D. Primetzhofer, L.P. Wang, J. Lu, L. Hultman, U. Jansson, Characterization of magnetron sputtered Cr-B and Cr-B-C thin films for electrical contact applications, Surf. Coat. Technol. 266 (2015) 167–176.

[25] C.H. Cheng, J.W. Lee, L.W. Ho, H.W. Chen, Y.C. Chan, J.G. Duh, Microstructure and mechanical property evaluation of pulsed DC magnetron sputtered Cr-B and Cr-B-N films, Surf. Coat. Technol. 206 (2011) 1711–1719.

[26] B. Mallia, M. Stüber, P.A. Dearnley, Character and chemical-wear response of high alloy austenitic stainless steel (Ortron 90) surface engineered with magnetron sputtered Cr-B-N ternary alloy coatings, Thin Solid Films 549 (2013) 216–223.

[27] J. Lin, J.J. Moore, W.C. Moerbe, M. Pinkas, B. Mishra, G.L. Doll, W.D. Sproul, Structure and properties of selected (Cr-Al-N, TiC-C, Cr-B-N) nanostructured tribological coatings, Int. J. Refract. Met. Hard Mater. 28 (2010) 2–14.

[28] K.P. Budna, J. Neidhardt, P.H. Mayrhofer, C. Mitterer, Synthesis-structure-property relations for Cr-B-N coatings sputter deposited reactively from a Cr-B target with 20 at% B, Vacuum 82 (2008) 771–776.

[29] Q.Z. Wang, Z.W. Wu, F. Zhou, J.W. Yan, Comparison of crack resistance between ternary CrSiC and quaternary CrSiCN coatings via nanoindentation, Mater. Sci. Eng. A 642 (2015) 391–397.

[30] Q. Ma, F. Zhou, Q.Z. Wang, Z.W. Wu, K.M. Chen, Z.F. Zhou, L. K-Y. Li, Influence of CrB2 target current on the microstructure, mechanical and tribological properties of Cr-B-C-N coatings in water, RSC Adv. 6 (2016) 47698-47711.

[31] W.C. Oliver, G.M. Pharr, An improved technique for determining hardness and elastic modulus using load and displacement sensing indentation experiments, J. Mater. Res. 7 (1992) 1564–1583.

[32] X. Cai, H. Bangert, Hardness measurements of thin films-determining the critical ratio of depth to thickness using FEM, Thin Solid Films 264 (1995) 59–71.

[33] C. Gamonpilas, E.P. Busso, On the effect of substrate properties on the indentation behaviour of coated systems, Mater. Sci. Eng. A 380 (2004) 52–61.

[34] M.E. Fitzpatrick, A.T. Fry, P. Holdway, F.A. Kandil, J. Shackleton, L. Suominen, Determination of Residual Stresses by X-Ray Diffraction-Issue 2, DTI, 2005, Measurement Good Practice Guide No. 52.

[35] Q. Luo, A.H. Jones, High-precision determination of residual stress of polycrystalline coatings using optimised XRD-$sin^2 \psi$ technique, Surf. Coat. Technol. 205 (2010) 1403–1408.

[36] A.G. Evans, E.A. Charles, Fracture toughness determinations by indentation, J. Am. Ceram. Soc. 59 (1976) 371–372.

[37] S. Zhang, X.M. Zhang, Toughness evaluation of hard coatings and thin films, Thin Solid Films 520 (2012) 2375–2389.

[38] S. Zhang, D. Sun, Q.Y.H.J. Du Fu, Toughness measurement of thin films: a critical review, Surf. Coat. Technol. 198 (2005) 74–78.

[39] Q.Z. Wang, F. Zhou, K.M. Chen, M.L. Wang, T. Qian, Friction and wear properties of TiCN coatings sliding against SiC and steel balls in air and water, Thin Solid Films 519 (2011) 4830–4841.

[40] T. Boll, M. Thuvander, S. Koch, J.N. Wagner, N. Nedfors, U. Jansson, K. Stiller, An APT investigation of an amorphous CrBC thin film, Ultramicroscopy 159 (2015) 217–222.

[41] C.Y. Guan, J.J. Zhao, F.C. Jia, C.Q. Zhuang, Y.Z. Bai, X. Jiang, Relationship between chemical compositions of magnetron sputtered B-C-N films and various experimental parameters, Vacuum 86 (2012) 1499–1504.

[42] H.Q. Wang, Q.G. Guo, J.H. Yang, Y. Zhao, X.L. Wang, Z.C. Tao, Z.J. Liu, Z.H. Feng, L. Liu, Microstructure and thermophysical properties of B_4C/graphite composites containing substitutional boron, Carbon 52 (2013) 10–16.

[43] C.Q. Zhuang, J.J. Zhao, F.C. Jia, C.Y. Guan, Z.L. Wu, Y.Z. Bai, X. Jiang, Tuning bond contents in B-C-N films via temperature and bias voltage within RF magnetron sputtering, Surf. Coat. Technol. 204 (2009) 713–717.

[44] Q.Z. Wang, Z.W. Wu, F. Zhou, H. Huang, K. Niitsu, J.W. Yan, Evaluation of crack resistance of CrSiCN coatings as a function of Si concentration via nanoindentation, Surf. Coat. Technol. 272 (2015) 239–245.

[45] M. Jirout, J. Musil, Effect of addition of Cu into ZrO_x film on its properties, Surf. Coat. Technol. 200 (2006) 6792–6800.

[46] J. Musil, M. Jirout, Toughness of hard nanostructured ceramic thin films, Surf. Coat. Technol. 201 (2007) 5148–5152.

[47] J. Blazek, J. Musil, P. Stupka, R. Cerstvy, J. Houska, Properties of nanocrystalline Al-Cu-O films reactively sputtered by DC pulse dual magnetron, Appl. Surf. Sci. 258 (2011) 1762–1767.

[48] J. Musil, R. Jílek, M. Meissner, T. Tölg, R. Čerstvý, Two-phase single layer Al-O-N nanocomposite films with enhanced resistance to cracking, Surf. Coat. Technol. 206 (2012) 4230–4234.

[49] J. Musil, J. Sklenka, R. Čerstvý, T. Suzuki, T. Mori, M. Takahashi, The effect of addition of Al in ZrO_2 thin film on its resistance to cracking, Surf. Coat. Technol. 207 (2012) 355–360.

[50] J. Musil, Hard nanocomposite coatings: thermal stability, oxidation resistance and toughness, Surf. Coat. Technol. 207 (2012) 50–65.

[51] Q.Z. Wang, F. Zhou, J.W. Yan, Evaluating mechanical properties and crack resistance of CrN, CrTiN, CrAlN and CrTiAlN coatings by nanoindentation and scratch Tests, Surf. Coat. Technol. 285 (2016) 203–213.

[52] J.M. Jungk, B.L. Boyce, T.E. Buchheit, T.A. Friedmann, D. Yang, W.W. Gerberich, Indentation fracture toughness and acoustic energy release in tetrahedral amorphous carbon diamond-like thin films, Acta Mater. 54 (2006) 4043–4052.

[53] C.M. Pecnik, D. Courty, D. Muff, R. Spolenak, Fracture toughness of esthetic dental coating systems by nanoindentation and FIB sectional analysis, J. Mech. Behav. Biomed. Mater. 47 (2015) 1–11.

[54] P.C. Wo, P.R. Munroe, Z.T. Jiang, Z.F. Zhou, K.Y. Li, Z.H. Xie, Enhancing toughness of CrN coatings by Ni addition for safety-critical applications, Mater. Sci. Eng. A 596 (2014) 264–274.

[55] Q.Z. Wang, F. Zhou, Z.F. Zhou, Y. Yang, C. Yan, C.D. Wang, W.J. Zhang, L.K.-Y. Li, I. Bello, S.-T. Lee, Influence of Ti content on the structure and tribological properties of Ti-DLC coatings in water lubrication, Diamond Relat. Mater. 25 (2012) 163–175.